Quaternary Research 79 (2013) 256–267

Contents lists available at SciVerse ScienceDirect

Quaternary Research

journal homepage: www.elsevier.com/locate/yqres

Long-term talus flatirons formation in the hyperarid northeastern Negev, Israel

Ronen Boroda [a,b,*], Ari Matmon [c], Rivka Amit [a], Itai Haviv [b], Naomi Porat [a], ASTERTeam [d], Dylan Rood [e], Yehuda Eyal [b], Yehuda Enzel [c]

[a] Geological Survey of Israel, 30 Malkhe Israel St., Jerusalem 95501, Israel
[b] Department of Geological and Environmental Sciences, Ben-Gurion University, Beer Sheva 84105, Israel
[c] The Fredy & Nadine Herrmann Institute of Earth Sciences, The Hebrew University of Jerusalem, Edmond J. Safra Campus Givat Ram, Jerusalem 91904, Israel
[d] M. Arnold, G. Aumaître, D. Bourlès, K. Keddadouche, CEREGE, UMR 6635 CNRS- Aix-Marseille University, BP 80, 13 545 Aix en Provence Cedex 4, France
[e] Lawrence Livermore National Laboratory, Livermore, CA 94550, USA

ARTICLE INFO

Article history:
Received 20 June 2012
Available online 15 January 2013

Keywords:
Talus flatirons
Landscape evolution
Hillslope
Cosmogenic nuclides
Numerical modeling
OSL
Hyperarid desert
Slope processes
Negev
Pleistocene

ABSTRACT

Colluvial sediments of talus relicts ("talus flatirons") around mesas preserve a record that sheds light on slope-forming processes at temporal scales $>10^3$ yr. The sedimentology and soil stratigraphy of two groups of talus flatirons in the northeastern hyperarid Negev desert reveal four deposition events in the younger talus and at least two in the older one. Numerical modeling of high-resolution ^{10}Be depth profiles suggests that these taluses were deposited during the middle Pleistocene; the younger talus group first depositional event occurred at 551 $^{+80}_{-142}$ ka and its abandonment occurred at 270 $^{+17}_{-38}$ ka. The abandonment of the older talus group and stabilization of its surface occurred at 497 $^{+176}_{-114}$ ka. These ages indicate that the development of the studied talus sequence is not specifically associated with Pleistocene glacial–interglacial cycles. The ^{10}Be modeled concentrations indicate significant differences in the average inheritance of talus flatirons of different groups. These differences can be attributed to variability in the transport distance and duration of gravel exposure during transport but could also reflect some temporal variability in cliff retreat. Our results also demonstrate that talus slopes in hyperarid areas, despite their steepness, can store sediment for long periods (~500 ka) and thus constitute a valuable archive.

Introduction

Talus slopes are common landforms in arid to hyperarid drainage basins and function as a primary storage reservoir of sediment close to its production sites. Their chronology, morphology, and sedimentology are intimately related to sediment production and flux from bedrock cliffs and its delivery into first- and larger-order fluvial systems. Talus slopes are therefore a key element in understanding basic questions regarding sediment production, storage, and transport. These slopes have a primary role in regulating drainage basin geomorphic responses to climate and environmental changes (e.g., Koons, 1955; Gerson and Grossman, 1987; Bull, 1991; Howard and Selby, 1994; Schmidt, 1994; Pederson et al., 2001; Anders et al., 2005; Enzel et al., in press). However, quantification of the processes which shape talus slopes at long-term temporal scales ($>10^3$) is still limited (Enzel et al., in press).

Talus relicts ("talus flatirons") are ubiquitous landforms of semiarid to hyperarid regions and are characterized by a concave longitudinal profile. Their apex is directed toward the source of the sediment, usually bedrock cliffs, while their distal part grades to a pediment and/or to fluvial terraces (e.g., Carson and Kirkby, 1972; Gerson, 1982; Gutiérrez and Martinez, 2001). It has been proposed that spatially well-organized generations of talus flatirons result from cycles of bedrock erosion, deposition of debris on slopes, and subsequent incision. The sequence of talus flatirons formed via the proposed cycles would be characterized by older talus flatirons that are systematically more distant from the cliff than the younger ones (e.g. Gerson, 1982; Gerson and Grossman, 1987; Schmidt, 1994; Gutiérrez et al., 2006; Boroda et al., 2011).

Over the last few decades most of the conceptual models of talus flatirons evolution were based on the analysis of these relicts in semiarid to hyperarid environments and have proposed changes in sediment production rates over time mainly in response to climatic changes (Everard, 1963; Gerson, 1982; Gerson and Grossman, 1987; Sancho et al., 1988; Bull, 1991; Arauzo et al., 1996; Schmidt, 1996; Gutiérrez et al., 1998, 2006). Most of these studies also assumed high rates of source cliff retreat during talus-sequence formation. Age estimations of talus flatirons were acquired using dating methods such as: cation ratios in desert

* Corresponding author at: Department of Geological and Environmental Sciences, Ben-Gurion University, Beer Sheva 84105, Israel.
E-mail address: Boroda@post.bgu.ac.il (R. Boroda).

0033-5894/$ – see front matter
http://dx.doi.org/10.1016/j.yqres.2012.11.012

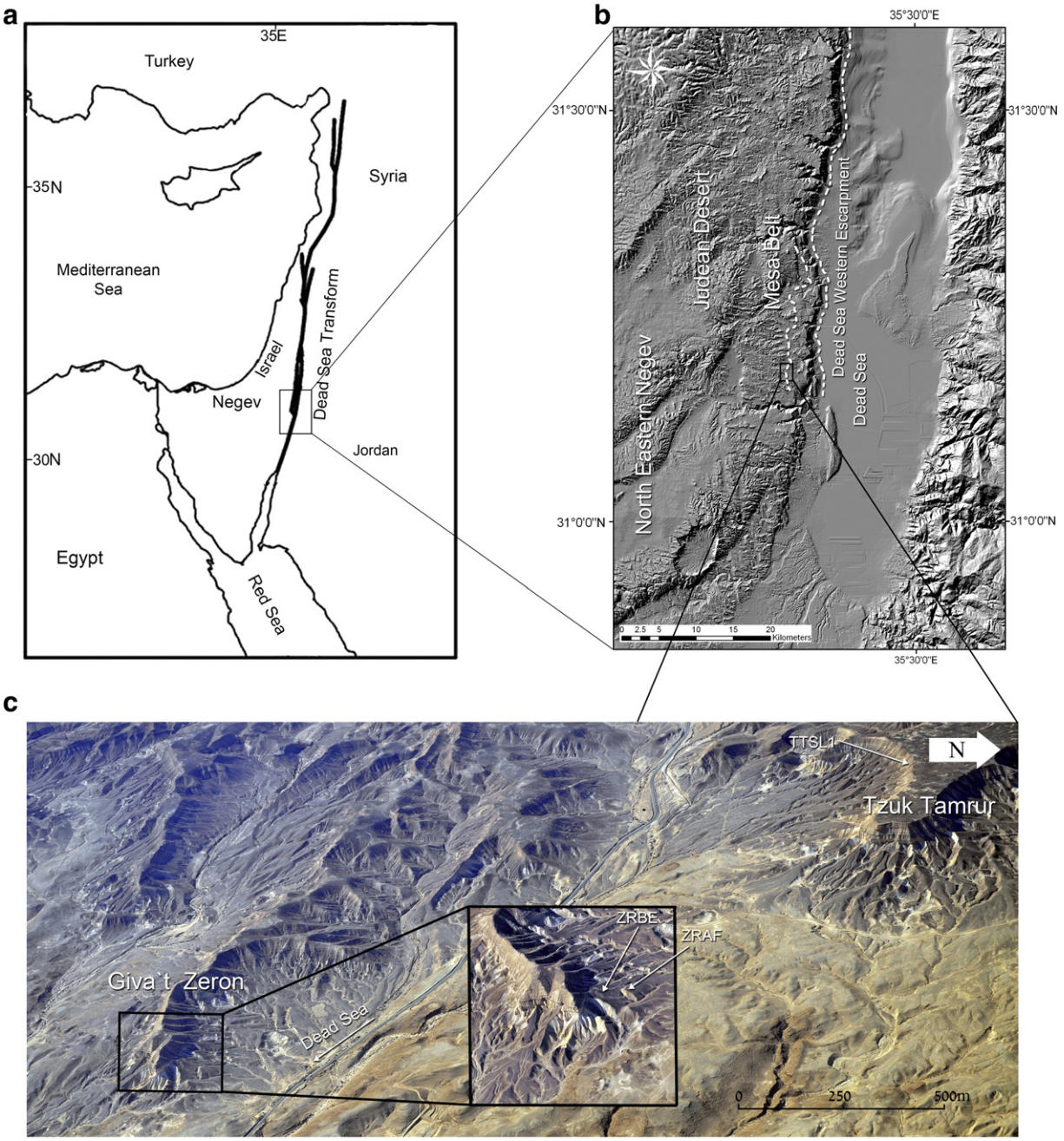

Figure 1. Study-area location (a) Location of the study area in the eastern Mediterranean region. (b) General topography of the study-area vicinity. Dashed lines indicate the location of the western escarpment of the Dead Sea basin and the mesa belt in the northeastern Negev and Judean desert. (c) A view of sequences of talus flatirons developed around Tzuk Tamrur and Giva't Zeron. The locations of the trenches are marked with white arrows. An enlargement of the Giva't Zeron area appears in the middle of the photo.

varnish (e.g. Gerson, 1982; Dorn, 1983), radiocarbon ages (e.g. Gutiérrez et al., 2006), and cosmogenic nuclide exposure ages (Boroda et al., 2011).

Recently, Boroda et al. (2011) studied three generations of talus flatirons in the northeastern Negev desert (Figs. 1, 2) and calculated simple exposure ages of the two oldest groups of talus flatiron using ^{10}Be concentration of the overlying desert pavement. In contrast to earlier studies that stressed retreat of the bedrock cliff as the main cause for the talus flatirons detachment from its source, Boroda et al. (2011) proposed that the distance separating talus flatirons from their respective source cliff is mainly gained by erosion and retreat of the talus apex away from the cliff and not by cliff retreat. However, the depositional processes, and temporal framework for talus flatirons formation were not described in detail in Boroda et al. (2011).

In the present study, we investigate the stratigraphy and soils of early to middle Pleistocene talus flatirons (groups A and B from Boroda et al., 2011), and analyze high-resolution depth profiles of in-situ cosmogenic radionuclides (e.g., Hancock et al., 1999; Matsushi et al., 2006; Nichols et al., 2006; Riihimaki et al., 2006; Matmon et al., 2009; Hidy et al., 2010; Guralnik et al., 2010) and optically stimulated luminescence (OSL) measurements. Then, we numerically model the cosmogenic nuclide concentrations to: (a) calculate exposure ages of the different depositional events

https://doi.org/10.1016/j.yqres.2012.11.012 Published online by Cambridge University Press

composing the talus flatiron and examine a possible correlation with Pleistocene glacial–interglacial climatic cycles, and (b) understand the process of sediment transport from the source cliff to the fluvial system. For this end, we use the modeled inheritance values of different units within a single talus slope as well as the modeled average inheritance values of different talus flatiron groups.

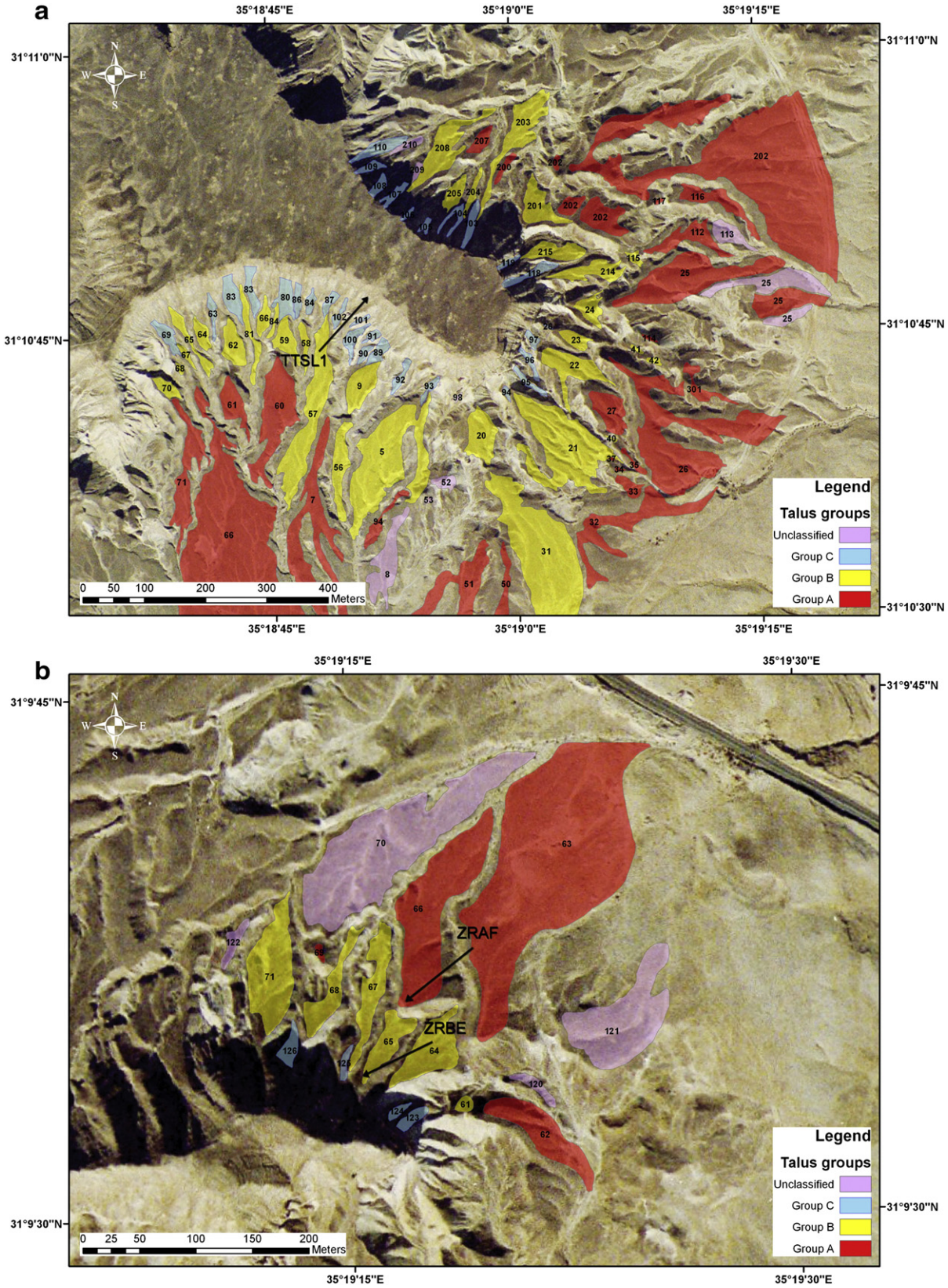

Figure 2. Morphostratigraphic maps of Tzuk Tamrur and Giva't Zeron. (a) Tzuk Tamrur site. Oldest talus group (red) is positioned at an average distance of 150 m from the source cliff; intermediate-age talus group (yellow) is positioned at an average distance of 30 m from the source cliff. Blue color represents the youngest talus group (connected to the cliff). Purple color represents unclassified taluses. (b) Giva't Zeron site. The color scheme is the same as in 2a. Locations of trenches at Giva't Zeron and sample TTSL1 are marked with black arrows.

https://doi.org/10.1016/j.yqres.2012.11.012 Published online by Cambridge University Press

Integrating new and previously published data (Boroda et al., 2011) from the study area enables a better understanding of the depositional history of talus flatiron cycles and transport processes of sediment on slopes in such hyperarid regions.

Study area

The study area is located in the hyperarid (mean annual rainfall <80 mm) northeastern Negev desert in Israel, along the western margins of the Dead Sea fault (Fig. 1). Exposed lithologies consist of horizontally bedded Turonian limestones, Santonian marls and chalks, and Campanian cherts. Significant channel downcutting during the late Cenozoic in the study area has caused the formation of mesas. Spatially, these mesas are positioned along a belt parallel to the Dead Sea western escarpment (Fig. 1b). These mesas are capped and maintained by the resistant chert of Mishash Formation, which overlies erodible chalk of Menuha Formation (Shaw, 1947; Boroda et al., 2011).

We investigate two mesas: Tzuk Tamrur and Giva't Zeron (Fig. 1; in Hebrew, Tzuk and Giva translate to “cliff” and “hill,” respectively). Tzuk Tamrur mesa is characterized by a flat chert top about 200 m wide, which ends in a bedrock cliff grading to a ~37° slope towards its base and the various talus groups. Giva't Zeron mesa is composed of a similar cliff but the flat-top mesa has been eroded and therefore, is narrower than in Tzuk Tamrur and only a few meters wide (Fig. 1c). Alternating phases of deposition and erosion led to the formation of three groups of talus flatirons with a systematic spatial distribution in which older talus flatirons are located farther from the source cliff than the younger ones. The oldest (red in Figs. 2, 3) and the intermediate-age (yellow in Figs. 2, 3) groups are detached from the source cliff by ~150 m and ~30 m, respectively (Boroda et al., 2011). The oldest talus flatiron group has maximum gradients ranging between 10° and 15° and the intermediate-age talus flatirons group has maximum gradients ranging between 16° and 20°.

Method

Sedimentological and pedological analyses

Two, ~3 m deep and 7–10 m long trenches reaching the bedrock and exposing the talus sediment-bedrock contact in the Giva't Zeron site were logged at 20:1 scale (trenches ZRAF and ZRBE on the oldest and intermediate-age talus groups, respectively (Figs. 1c, 2b, 3)). One wall in each trench was mapped in detail to delineate sedimentary contacts, unconformities, buried soils, and soil horizons within the talus deposit. The soils were classified according to Dan et al. (1964), Soil Survey Staff (1975), and Birkeland (1999). Additional pedogenic features specific to hyperarid desert environments were documented according to Amit and Gerson (1986) and Amit et al. (1993).

Geochronology

Two dating methods were applied to determine the depositional history of the different talus groups: optically stimulated luminescence (OSL, Aitken, 1998), and in-situ produced cosmogenic nuclide exposure dating (e.g., Lal, 1991; Bierman and Turner, 1995; Gosse and Phillips, 2001).

Optically stimulated luminescence (OSL) measurements

Ten sediment samples, five from the oldest group and five from the intermediate-age talus group, were collected from the stratigraphic units exposed in the trench walls. These samples range in depth from just below the surface at the top to the talus-bedrock contact at the bottom (Fig. 4). Fine sand-size quartz grains (63–125 or 74–125 μm) were extracted from the sediments using routine laboratory procedures (Porat, 2007). OSL measurements were carried out on a Risø DA-12 TL/OSL reader on a limited number of aliquots (4–5). The equivalent doses (De) were determined by using the OSL

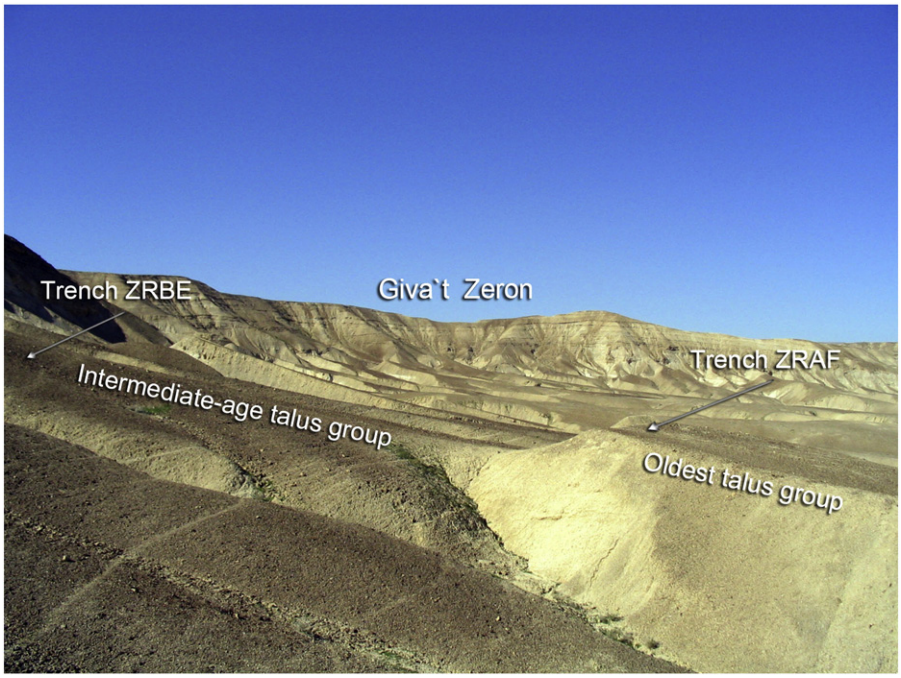

Figure 3. Talus flatirons sequence in Giva't Zeron: Oldest talus flatiron group (location of trench ZRAF) on the right has a maximum gradient ranging between 10° and 15°. Intermediate-age talus flatirons group (location of trench ZRBE) on the left has a maximum gradient ranging between 16° and 20°. Trenches locations are marked with gray arrows.

https://doi.org/10.1016/j.yqres.2012.11.012 Published online by Cambridge University Press

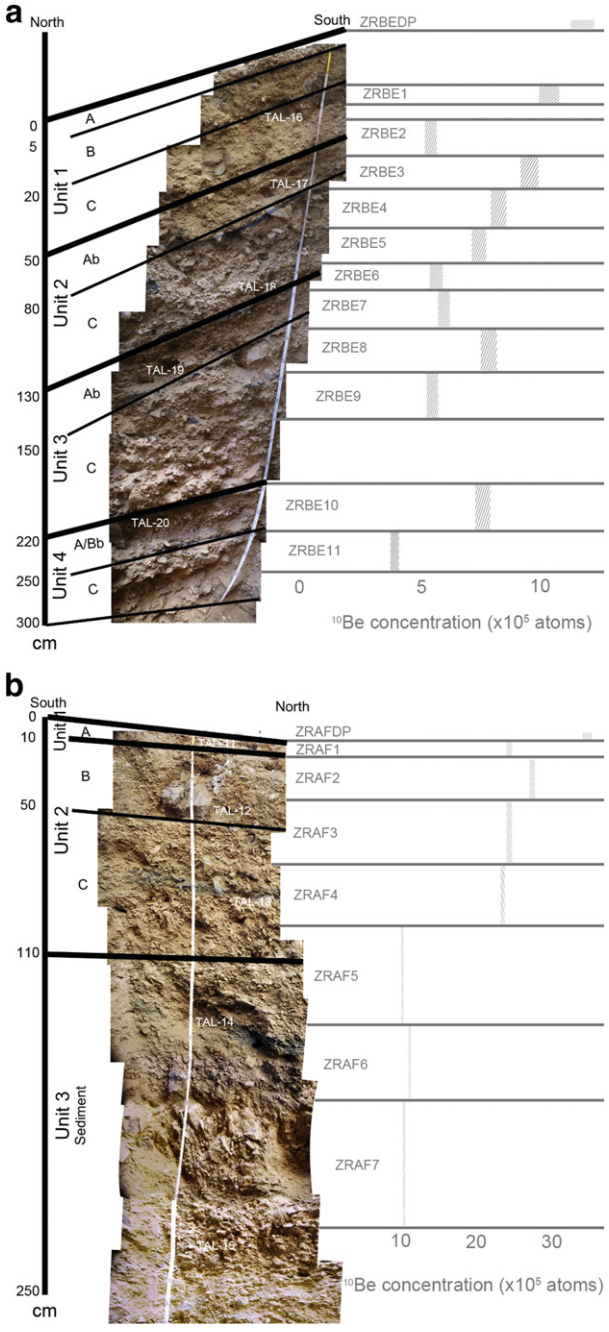

Figure 4. Sedimentary and soil profiles exposed in trenches excavated on the talus groups. (a) Eastern wall of trench ZRBE (intermediate-age talus group). (b) Western wall of trench ZRAF (oldest talus group). Each soil horizon in the columnar section is marked by a black line and accepted symbols. The different sedimentary units inferred to have been deposited at different depositional events are separated by bold black lines and symbols. The location of cosmogenic samples and their ^{10}Be concentrations (in 10^5 atoms g^{-1} quartz with 1σ analytical error) are marked by gray lines and squares. ^{10}Be concentrations generally decrease with increasing depth for each of the sedimentary units. The locations of the OSL samples are marked by white symbols. The identification of Unit 1 of trench ZRAF is based only on the step in the ^{10}Be concentrations without any correlating field evidence.

signal and the standard single-aliquot regenerative dose (SAR) protocol (Murray and Wintle, 2000).

^{10}Be measurements

Cosmogenic nuclides such as ^{10}Be and ^{26}Al are produced in measurable amounts in the uppermost few meters of exposed rock, sediment, and soil; thus, they are a sensitive monitor of near-surface residence time. This technique allows calculations of exposure ages and/or erosion rates over various time scales at various geomorphic setting (e.g., Bierman and Turner, 1995; Small et al., 1999). When a depositional surface is abandoned, an exponential cosmogenic profile will evolve since production rates decay with depth (Lal and Arnold, 1985; Phillips et al., 1998; Hidy et al., 2010). The depth distribution of concentrations of cosmogenic nuclides in amalgamated sediment samples has been previously used for estimating exposure ages, rates of erosion or aggradation, and inherited cosmogenic nuclide concentrations in a variety of geomorphic settings (e.g. Hancock et al., 1999; Perg et al., 2001; Brocard et al., 2003; Braucher et al., 2009; Matmon et al., 2009; Hidy et al., 2010; Guralnik et al., 2010). One of the goals of the depth profile procedure is to separate nuclide inheritance from post-depositional nuclide production, thereby permitting accurate surface exposure dating of sediments.

Twenty samples were collected from trenches at Giva't Zeron for cosmogenic nuclide analysis (Figs. 1c, 2b, 4): eleven from the intermediate-age talus group (trench ZRBE), seven from the oldest talus group (trench ZRAF) and two samples of at least 100 amalgamated desert pavement clasts from the surface of each talus group. We use this analysis to estimate: (a) the depositional history of the oldest and intermediate-age talus groups and (b) the sediment-transport pattern based on the average cosmogenic inheritance.

One sample of amalgamated bedrock from interfluves between rills (sample TTSL1) was collected above the talus-flatiron apex at Tzuk Tamrur (Figs. 1c, 2a). This sample was used to compare the rate of cliff retreat at Tzuk Tamrur to that of Giva't Zeron.

Samples were processed at the Cosmogenic Isotope Laboratory at the Hebrew University, Jerusalem, following the procedure by Bierman and Caffee (2001). Analyses were performed at the accelerator mass spectrometry (AMS) facilities at Lawrence Livermore National Laboratory (LLNL), USA, and ASTER, CEREGE, France. Samples measured at LLNL are normalized to the AMS standard KNSTD3110 with a ^{10}Be/^{9}Be ratio value of 2.85×10^{-12}. Samples measured at CEREGE are normalized to NIST standard with a ^{10}Be/^{9}Be ratio value of 2.79×10^{-11}. The reported concentrations are comparable.

Numerical modeling

Profile model exposure ages were calculated using Eq. (1) (Brown et al., 1998):

$$N = \frac{P(z)}{\rho\varepsilon\Lambda^{-1}+\lambda}\left(1-e^{-(\rho\varepsilon\Lambda^{-1}+\lambda)t*}\right)+N(0)e^{-\lambda t*} \quad (1)$$

where N is the measured concentration of the cosmogenic nuclide in atoms g^{-1} quartz, P is the total surface production rate of the cosmogenic nuclide in atoms g^{-1} quartz yr^{-1}, ρ is the density of the consolidated sediment (2.4 g cm^{-3}), ε is the erosion rate of the surface in cm yr^{-1}, Λ is the attenuation depth of neutrons (165 g cm^{-2}), t^* is the exposure time in years between colluvial unit deposition and burial by subsequent colluvial unit, $N(0)$ is the inherited cosmogenic nuclide concentration in atoms g^{-1} quartz at the time of deposition, and λ is the cosmogenic nuclide decay constant (4.99×10^{-7} yr^{-1}). We use a ^{10}Be half-life value of 1.387 ± 0.012 Ma (Korschinek et al., 2010) for all age and erosion calculations. In converting concentrations to exposure time, we adopt the latitude and altitude scaling factors of Stone (2000) and correspondingly reduce the previous accepted, spallation, sea-level high-latitude reference production rate of 4.96 atoms g^{-1} yr^{-1} (Table 6 in Balco et al., 2008) by a factor of 1.106 (Nishiizumi et al., 2007) to give $P_1 = 4.49$ ^{10}Be atoms g^{-1} yr^{-1}, which accounts for the renormalization of AMS calibration standard reference materials. Production by muons followed the procedure described in Granger and Smith (2000). Decrease in production with

https://doi.org/10.1016/j.yqres.2012.11.012 Published online by Cambridge University Press

depth by fast neutrons or by muon capture was calculated using the formulation of Granger and Muzikar (2001).

We set the exposure time (t^*) and the inheritance $N(0)$ as free parameters (one value for each parameter for all the samples composing a depositional event). Erosion (ε) was neglected due to the preservation of soil horizons in stratigraphic units and the extreme resistance of pebble-size chert clasts in desert pavements to erosion in this hyperarid environment (Matmon et al., 2009; Guralnik et al., 2010; Boroda et al., 2011). The model objective was to estimate the exposure time (t*) and inheritance $N(0)$ of each unit by minimizing the misfit between the measured and predicted concentrations. Material constituting the deposit has been emplaced over a short period of time, several ka, with respect to the subsequent duration of exposure. Predicted ^{10}Be concentrations (Np) were compared with the measured concentrations (Nm) for all the samples in each scenario. The misfit function was expressed using a chi-square test (Bevington and Robinson, 2003). The level of fit was calculated using Eq. (2):

$$\chi^2 = \frac{(Np_1 - Nm_1)^2}{\sigma_{m_1}^2} + \frac{(Np_2 - Nm_2)^2}{\sigma_{m_2}^2} + \ldots \frac{(Np_n - Nm_n)^2}{\sigma_{m_n}^2} \quad (2)$$

The two profiles in the study area are complex profiles because they result from more than one depositional event. Thus, we apply the model to find the best fit for the entire profile which yields the optimized t* and $N(0)$ for each unit (i.e. the number of free model parameters for a defined best fit value is the number of depositional events multiplied by 2). The model principals are as follows: The exposure time (t*) and inheritance $N(0)$ of the first depositional event (lowest/oldest unit) are calculated considering the upper part of the unit as the paleo-surface. The exposure time and inheritance for the second depositional event are calculated the same way as the underlying unit but considering the upper part of the new unit as the new paleo-surface. As the cosmogenic depth profile for the new unit is built, the cosmogenic depth profile for the underlying unit continues to be built but considering the upper new unit as the paleo-surface. This process continues throughout the profile to give the optimized t* and $N(0)$ for each of the depositional units composing the profile.

We performed $>10^9$ model runs and applied a global minimum search algorithm to identify the best-fit scenario. We present the solution space with an error cutoff of 5% for the minimum chi-square indicating the preferred range of values for each free parameter.

Results

Sedimentary characteristics of the talus-flatiron sequence

Intermediate-age talus group (trench ZRBE)

Sedimentary and soil characteristics in the ZRBE profile indicate the presence of four colluvial units associated with three buried soils in addition to the surface soil (Fig. 4a). The surface of the talus flatiron is covered (>85%) by a well-developed desert pavement and is barren of vegetation. Soil morphologic and key sedimentary features for these four units are as follows: (a) Unit 1 (upper soil profile): A horizon (0–5 cm depth) mostly fine sand and silt, B horizon (5–20 cm depth) with <20% highly angular gravel (2–3 cm) weakly cemented by gypsum, C horizon (20–50 cm depth) well-sorted grain-supported clasts (>70% clasts, 2–3 cm) and weak gypsum cementation and a clear lower boundary, (b) Unit 2 (paleosol 1): Ab (buried A horizon, 50–80 cm depth) unsorted grain-supported clasts (>60% clasts, ~10 cm) with gypsum cementation, C horizon (80–130 cm depth) of stratified grain-supported clasts (>90% clasts, 1–2 cm) with weak gypsum cementation and sharp lower boundary, (c) Unit 3 (paleosol 2): Ab (130–150 cm depth) grain-supported clasts, poorly cemented by gypsum, C horizon (150–220 cm depth) stratified grain-supported clasts (4–5 cm) weakly cemented by gypsum and clear lower boundary and (d) Unit 4 (paleosol 3): A/Bb (220–250 cm depth) grain-supported clasts (3–4 cm) weakly cemented by gypsum and C (250–300 cm depth) composed of well stratified grain-supported clasts (> 80%, 4–5 cm) also weakly cemented.

Oldest talus group (trench ZRFA)

Sedimentary and soil characteristics in ZRAF profile reveal that this profile is composed of at least two colluvial units (Fig. 4b). The surface is covered (>85%) by a well-developed desert pavement (3–5 cm diameter platy clasts) and it is barren of vegetation. Soil morphologic and key sedimentary features for these two units are as follows: (a) an upper soil profile (marked as the combined units 1 and 2 in Fig. 4b): A horizon (0–10 cm depth) mostly fine sand and silt, B horizon (10–50 cm depth) with 50% shuttered gravel and abundant gypsum crystals, and C horizon (50–110 cm depth) grain supported clasts (>80%, ~5 cm) with a sharp lower boundary (b) a lower sediment (unit 3 in Fig. 4b): 240-cm-thick unit of the colluvial material. Soil development was not observed in this unit.

Optically stimulated luminescence (OSL) ages

The OSL ages range between 11 ± 10 and 138 ± 39 ka for the intermediate-age talus group and between 22 ± 5 and 99 ± 26 ka for the oldest talus group (Table 1, Fig. 4). Within each talus group ages increase with depth. The overall age ranges for the youngest and oldest fine dust materials in both talus units are essentially the same, given the overlapping analytical uncertainty associated with the dates. The OSL results show that the D_e values are high (50–220 Gy), perhaps due to the high dose rate. This suggests that the OSL signal may be close to saturation and that the ages are underestimated.

Cosmogenic nuclide exposure ages

In both depth profiles the concentrations of ^{10}Be generally decrease with depth (Table 2, Figs. 4, 5). The concentrations in profile ZRAF (oldest talus group) are significantly higher than those in profile ZRBE (intermediate-age talus group) (Fig. 5). Desert pavement samples yielded $1.12 \pm 0.042 \times 10^6$ and $3.33 \pm 0.095 \times 10^6$ ^{10}Be atoms g^{-1}, for the intermediate-age and oldest talus groups, respectively. These concentrations correspond to simple exposure ages of ~253 ka and ~870 ka, respectively, assuming $N(0) = 0$ and $\varepsilon = 0$. The ZRBE ^{10}Be depth profile presents three pronounced steps, each characterized by relatively high concentration and lower values above and below (Figs. 4, 5). For example, sample ZRBE3 (60–80 cm depth) yielded $0.93 \pm 0.032 \times 10^6$ ^{10}Be atoms g^{-1} with lower concentration of $0.57 \pm 0.02 \times 10^6$ and $0.82 \pm 0.029 \times 10^6$ ^{10}Be atoms g^{-1} for samples ZRBE2 (40–60 cm depth) and ZRBE4 (80–100 cm depth), respectively. Profile ZRAF shows two such steps (Figs. 4, 5). For example, sample ZRAF2 (12–40 cm depth) yielded $2.74 \pm 0.068 \times 10^6$ ^{10}Be atoms g^{-1} with lower concentrations of $2.36 \pm 0.063 \times 10^6$ and $2.37 \pm 0.07 \times 10^6$ ^{10}Be atoms g^{-1} for samples ZRAF1 (0–12 cm depth) and ZRAF3 (40–70 cm depth), respectively. Sample TTSL1 from Tzuk Tamrur yielded a ^{10}Be concentration of $0.03 \pm 0.006 \times 10^6$ atoms g^{-1}, which is similar to samples from the same morphologic position at Giv'at Zeron (samples ZRSL1 and ZRSL2; Boroda et al., 2011).

Discussion

Ages of talus flatiron depositional events

Numerical modeling of cosmogenic nuclide depth profiles can solve for exposure age and/or inheritance variation in a complex

https://doi.org/10.1016/j.yqres.2012.11.012 Published online by Cambridge University Press

Table 1
OSL results of samples collected from trenches ZRBE and ZRAF along talus flatirons around Giva't Zeron mesa.

Sample	Trench	Depth (m)	K (%)	U (ppm)	Th (ppm)	Ext. α (μGy yr^{-1})	Ext. β (μGy yr^{-1})	Ext. γ (μGy yr^{-1})	Cosmic (μGy yr^{-1})	Total dose (μGy yr^{-1})	De (Gy)	Age (ka)
TAL-11	ZRAF	0.1	0.15	16.6	0.9	49	1912	2269	264	4494 ± 52	50 ± 46	11 ± 10
TAL-12	ZRAF	0.4	0.21	10.3	1.1	31	1239	1502	219	2991 ± 63	201 ± 110	67 ± 37
TAL-13	ZRAF	0.8	0.16	8.6	0.6	26	1016	1235	190	2467 ± 61	186 ± 31	75 ± 31
TAL-14	ZRAF	1.4	0.24	7.3	1	22	910	1133	176	2241 ± 60	309 ± 88	138 ± 39
TAL-15	ZRAF	2.3	0.09	9.3	0.5	28	1072	1275	158	2532 ± 37	220 ± 112	89 ± 44
TAL-16	ZRBE	0.2	0.21	9.5	1.3	29	1160	1403	243	2835 ± 64	62 ± 13	22 ± 5
TAL-17	ZRBE	0.7	0.19	11.4	0.9	34	1347	1625	196	3201 ± 65	140 ± 36	44 ± 11
TAL-18	ZRBE	1.1	0.13	9.8	0.7	29	1146	1372	183	2731 ± 62	149 ± 63	55 ± 23
TAL-19	ZRBE	1.5	0.2	8.4	1	25	1022	1247	174	2468 ± 61	150 ± 41	61 ± 17
TAL-20	ZRBE	2.2	0.12	7.5	0.4	22	876	1061	160	2119 ± 61	209 ± 55	99 ± 26

Gamma + cosmic dose rates were measured in the field using a portable gamma spectrometer.
Grain size for all samples was 75–125 μm.
Gamma was calculated from the radioactive elements and the cosmic dose was estimated from burial depth.
Water contents estimated at 2 ± 1%.

sedimentary profile (e.g. Phillips et al., 1998; Hancock et al., 1999; Nichols et al., 2002, 2006; Riihimaki et al., 2006; Matmon et al., 2009; Guralnik et al., 2010). In most of these studies, this method was applied to delineate sedimentary contacts. For example, Phillips et al. (1998) illustrated the ability of cosmogenic nuclide depth profiles to locate subtle unconformities in alluvial sequences in stream terraces and an alluvial fan. They showed that an anomalously high concentration of ^{21}Ne from the deepest sample probably represents the unconformable contact of an older alluvial sequence with a higher nuclide inheritance. Matmon et al. (2009) reconstructed a three-step history of clastic and eolian deposition on the Paran Plains of the Negev using ^{10}Be concentration profile and suggested that sediment was deposited in two or more cycles and not in a single depositional event.

The integration of sedimentary and soil stratigraphy data with the cosmogenic nuclides depth profiles in this study reveals that the pattern of ^{10}Be concentrations is mostly in agreement with field observations (Fig. 4). This agreement supports the reliability of the model. The sediment and soil-stratigraphy of the intermediate-age talus group (profile ZRBE) indicate deposition of four colluvial units separated by intervals of soil development and minor sediment accretion in between. The cosmogenic nuclide concentrations of the samples within each unit show an exponential decrease in concentrations with depth. Each unit is separated from the lower and upper units by discontinuities in the cosmogenic nuclide concentration profile that correspond to the unconformities in the sequence represented by the buried soils.

Moreover, the stratigraphy, sedimentology, and concentrations of ^{10}Be as revealed in ZRBE and ZRAF trenches lead to the following assumptions: (a) each single colluvial unit was emplaced over a short period of time, several ka, with respect to the subsequent duration of exposure. Thus, the concentrations of ^{10}Be in each colluvial unit decrease with depth (b) there was negligible erosion of the surface layer between successive depositional events as evidenced by the soil profiles and the general existence of an exponential profile of cosmogenic isotope concentrations in each unit. Absence of the upper part of a cosmogenic depth profile would have pointed to a layer that was stripped prior to the deposition of the subsequent layer (Nichols et al., 2005; Riihimaki et al., 2006). (c) Following the deposition of the uppermost colluvial unit, the

Table 2
Raw cosmogenic ^{10}Be data of samples from the Giva't Zeron and Tzuk Tamrur study sites.

Sample	Trench	Location [°N/°W]	Elevation [m asl]	Depth [cm]	Thickness [cm]	Total production rate [atoms g^{-1} yr^{-1}]	Shielding factor	Quartz[a] [g]	Carrier solution[b] [g]	^{10}Be/^{9}Be[cd] [×10^{-13}]	^{10}Be concentration[e] [10^6 atoms g^{-1} SiO$_2$]
ZRAFDP	ZRAF	31.1605/35.3215	86	0	1	4.41	1	20.001	0.308	32.55 ± 0.66	3.33 ± 0.095
ZRAF1	ZRAF	31.1605/35.3215	86	0-12	1	3.73	1	30.038	0.306	34.86 ± 0.62	2.36 ± 0.063
ZRAF2	ZRAF	31.1605/35.3215	86	12-40	1	2.46	1	30.008	0.309	39.99 ± 0.59	2.74 ± 0.068
ZRAF3	ZRAF	31.1605/35.3215	86	40-70	1	1.69	1	30.011	0.306	34.90 ± 0.76	2.37 ± 0.070
ZRAF4	ZRAF	31.1605/35.3215	86	70-100	1	1.08	1	34.996	0.308	39.46 ± 0.57	2.31 ± 0.057
ZRAF5	ZRAF	31.1605/35.3215	86	100-145	1	0.67	1	34.998	0.307	17.48 ± 0.36	1.01 ± 0.029
ZRAF6	ZRAF	31.1605/35.3215	86	145-180	1	0.46	1	35.005	0.308	19.57 ± 0.35	1.14 ± 0.031
ZRAF7	ZRAF	31.1605/35.3215	100	180-225	1	0.25	1	39.57	0.309	19.44 ± 0.27	1.00 ± 0.025
ZRBEDP	ZRBE	31.1600/35.3211	100	0	1	4.40	1	20.016	0.305	11.24 ± 0.32	1.12 ± 0.042
ZRBE1	ZRBE	31.1600/35.3211	100	20-30	1	3.11	1	25.011	0.298	12.77 ± 0.36	1.00 ± 0.035
ZRBE2	ZRBE	31.1600/35.3211	100	40-60	1	2.20	1	25.039	0.298	73.83 ± 0.21	0.57 ± 0.02
ZRBE3	ZRBE	31.1600/35.3211	100	60-80	1	1.69	1	30.008	0.296	14.32 ± 0.4	0.93 ± 0.032
ZRBE4	ZRBE	31.1600/35.3211	100	80-100	1	1.30	1	30.092	0.298	12.54 ± 0.36	0.82 ± 0.029
ZRBE5	ZRBE	31.1600/35.3211	100	100-120	1	1.01	1	30.025	0.299	11.43 ± 0.32	0.75 ± 0.026
ZRBE6	ZRBE	31.1600/35.3211	100	120-140	1	0.79	1	35.014	0.297	10.62 ± 0.33	0.59 ± 0.022
ZRBE7	ZRBE	31.1600/35.3211	100	140-160	1	0.59	1	35.009	0.298	10.92 ± 0.37	0.62 ± 0.024
ZRBE8	ZRBE	31.1600/35.3211	100	160-180	1	0.47	1	35.012	0.3	13.71 ± 0.41	0.78 ± 0.028
ZRBE9	ZRBE	31.1600/35.3211	100	180-200	1	0.39	1	35.028	0.301	10.13 ± 0.31	0.58 ± 0.027
ZRBE10	ZRBE	31.1600/35.3211	100	240-260	1	0.25	1	35.019	0.301	13.25 ± 0.38	0.76 ± 0.027
ZRBE11	ZRBE	31.1600/35.3211	100	260-280	1	0.24	1	35.04	0.299	7.74 ± 0.22	0.44 ± 0.015
TTSL1	Surface	31.1794/35.3152	171	0	1	4.07	1	25.055	0.295	0.64 ± 0.08	0.03 ± 0.006

[a] A density of 2.4 g cm^{-3} was used based on the chert composition of the profile samples excluding TTSL1 (2.65 g cm^{-3}, based on chert density).
[b] Carrier solution Be concentration is 974 ppm with an average ^{10}Be/^{9}Be ratio of 2*10^−14.
[c] Isotope ratios were normalized to ^{10}Be standards with a value of 2.85 × 10^{-12} and 2.79 × 10^{-11} at LLNL and CEREGE respectivaly using a ^{10}Be half-life of 1.387 × 10^6 yr.
[d] Uncertainties are reported at the 1σ confidence level.
[e] Propagated uncertainties include error in the blank, carrier mass (1%), and counting statistics.

https://doi.org/10.1016/j.yqres.2012.11.012 Published online by Cambridge University Press

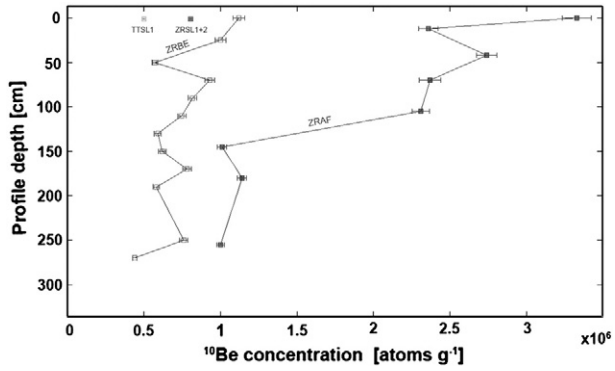

Figure 5. Distribution of cosmogenic nuclide concentrations with depth for the intermediate-age talus group (profile ZRBE) and for the oldest talus group (profile ZRAF). Notice the general higher concentrations in the oldest talus group. The two samples from the cliff face of Giva't Zeron (ZRSL1 and ZRSL2; Boroda et al., 2011) are marked on the upper left side of the graph.

talus sediment stabilized and a desert pavement composed of chert clasts which experience negligible erosion was developed (Matmon et al., 2009; Guralnik et al., 2010; Boroda et al., 2011), and (d) variation in the inheritance within a single colluvial unit is unlikely due to the proximity of the samples to the sediment source, 30 and 150 m from the sampling sites of trenches ZRBE and ZRAF, respectively.

The best-fit model out of 10^9 simulations yielded a minimum chi-squared value of 8.65 (Table 3). Based on this model: (a) the first depositional event in the intermediate-age talus group occurred at 551 $^{+80}_{-142}$ ka, and (b) the abandonment of the intermediate-age talus group and stabilization of its surface occurred at 270 $^{+17}_{-38}$ ka (Figs. 6, 7a). Considering the complex stratigraphy of the sequence (which includes four depositional units) the model yields a reasonable chi-square value. Previously published studies have yielded similar chi-square values. For example, modeling results for fluvial terrace at Lees Ferry, Arizona (Hidy et al., 2010), yielded ages at an ~10^5 yr time scale with converging pattern similar to this study and chi-square values between 15 and 20. The converging pattern of the deposition age as a function of the chi-square value is good (Fig. 8). The envelope of the results has a low gradient, which means that any change in the age relative to the optimum has a significant penalty in the chi-square value.

The stratigraphy of the oldest talus group (trench ZRAF) reveals two colluvial units based on textural variation in the profile (marked as combined units 1 + 2 and unit 3 in Fig. 4b). No buried soil was detected in between. This may indicate that either deep stripping of unit 3 occurred prior to the deposition of the upper unit or that the time interval between the two depositional events was too short for a soil to develop. Unlike profile ZRBE, the depositional history, based on field observations, does not fully correspond with the distribution of ^{10}Be concentrations with depth (Fig. 4b). The contact between units 2 and 3 at a depth of 110 cm agrees well with the unconformity in the cosmogemic nuclides concentration. However, the upper unconformity between units 1 and 2 is based on the cosmogenic data alone and is not visible in the field. We applied the model only for units 1 and 2 due to possible stripping of unit 3. Based on the best-fit model of 10^9 simulations (Table 3) the abandonment of the oldest talus group and stabilization of its surface occurred at 497 $^{+176}_{-114}$ ka (Figs. 6, 7a). Although overlapping ages of the abandonment of the oldest talus and initial deposition of the intermediate-age talus groups were obtained (Fig. 7a), the observed stratigraphy requires that both groups were not deposited at the same time. The oldest talus group is topographically higher than the intermediate-age talus group. Our age results demonstrate that talus flatirons in arid areas, despite their steepness, can store sediment for long periods (~500 ka) and thus constitute a valuable archive.

Talus sediment transport process

The modeled cosmogenic depth profile of the intermediate-age talus group (trench ZRBE), yield a minimum chi-squared value of 8.65, when variability in the inheritance with depth is allowed (i.e. one value for all samples within a unit but allowing different values for different units composing the profile) (Table 3, black line in Fig. 9a). The model yields large variation in the inherited concentrations of ^{10}Be with depth with the lowest value being 20 $^{+51}_{-14}\times10^3$ atoms g^{-1} in unit 4 and the highest value being 540 $^{+0}_{-105}\times10^3$ atoms g^{-1} in unit 2 (Fig. 7b). In comparison, a somewhat higher chi-square value (12.53) is obtained when variability in the inheritance with depth is not allowed (i.e. one value for all samples composing the profile) (Table 3; dashed line in Fig. 9a), and is set to an average inheritance value of 349 $^{+27}_{-151}\times10^3$ atoms g^{-1}. A similar trend is also observed for the oldest talus group (trench ZRAF): when variability in the inheritance with depth is allowed (Table 3, black line in Fig. 9b), the model results yield a minimum chi-squared value of 6.42. In comparison, when variability in the inheritance with depth is not allowed (Table 3; dashed line in Fig. 9b), a higher chi-square value of 7.83 is obtained. These results suggest that variability in inherited values is more likely than uniform inheritance.

To test whether the model is sensitive to the difference between the average inheritance of the two talus groups we have calculated model ages of the intermediate-age talus profile, while applying the average inheritance of the oldest talus group profile and vise-versa. This modeling scenario yielded much higher chi-square values (Table 3; gray line in Figs. 9a and b). These high values support the conclusion that the inheritance within the older talus group is much higher (Fig. 7b). A similar trend of increasing inheritance values with sediment age was noted by Hancock et al. (1999) in a sequence of terraces in the Wind River, Wyoming. The higher modeled average

Table 3
Best-fit model results for deposition age and inheritance of each depositional unit.

Talus group	Model scenarios	Deposition age (ka) [d]				Inheritance ($\times10^3$ atoms g^{-1}) [d]				Chi-square
		Unit 1	Unit 2	Unit 3	Unit 4	Unit 1	Unit 2	Unit 3	Unit 4	
Intermediate-age (trench ZRBE)	Variability in inheritance is allowed[a]	270 $^{+17}_{-38}$	289 $^{+41}_{-49}$	444 $^{+55}_{-129}$	551 $^{+80}_{-142}$	68 $^{+106}_{-12}$	540 $^{+0}_{-105}$	69 $^{+273.5}_{-4.7}$	20 $^{+51}_{-14}$	8.65
	Variability in inheritance is not allowed[b]	175 $^{+56}_{-3}$	283 $^{+98}_{-15}$	359 $^{+130}_{-43}$	399 $^{+173}_{-52}$	349 $^{+27}_{-151}$	349 $^{+27}_{-151}$	349 $^{+27}_{-151}$	349 $^{+27}_{-151}$	12.53
	Applying inheritance from the other group[c]	605 $^{+218}_{-579}$	713 $^{+427}_{-684}$	811 $^{+552}_{-782}$	866 $^{+649}_{-836}$	2174 $^{+164}_{-121}$	2174 $^{+164}_{-121}$	2174 $^{+164}_{-121}$	2174 $^{+164}_{-121}$	227.72
Oldest (trench ZRAF)	Variability in inheritance is allowed[a]	497 $^{+176}_{-114}$	498 $^{+237}_{-114}$			1166 $^{+333}_{-587}$	2218 $^{+99}_{-142}$			6.42
	Variability in inheritance is not allowed[b]	189 $^{+60}_{-56}$	356 $^{+176}_{-160}$			2174 $^{+164}_{-121}$	2174 $^{+164}_{-121}$			7.83
	Applying inheritance from the other group[c]	749 $^{+113}_{-113}$	1775 $^{+423}_{-386}$			349 $^{+27}_{-151}$	349 $^{+27}_{-151}$			17.7

A 5% cutoff from the minimum chi-squared value was used to calculate the error range.
[a] The model includes 8 and 4 free parameters for the intermediate-age and oldest talus groups respectively.
[b] All inheritance parameters are equal ($N(0)_1 = N(0)_2 = N(0)_n$). The model includes 5 and 3 free parameters for the intermediate-age and oldest talus groups respectively.
[c] The model includes 5 and 3 free parameters for the intermediate-age and oldest talus groups respectively.
[d] Notice that the deposition age (t) refers to the time between deposition and the present. This is different than t* (see Eq. (1)) which refers to the time between deposition and subsequent burial.

https://doi.org/10.1016/j.yqres.2012.11.012 Published online by Cambridge University Press

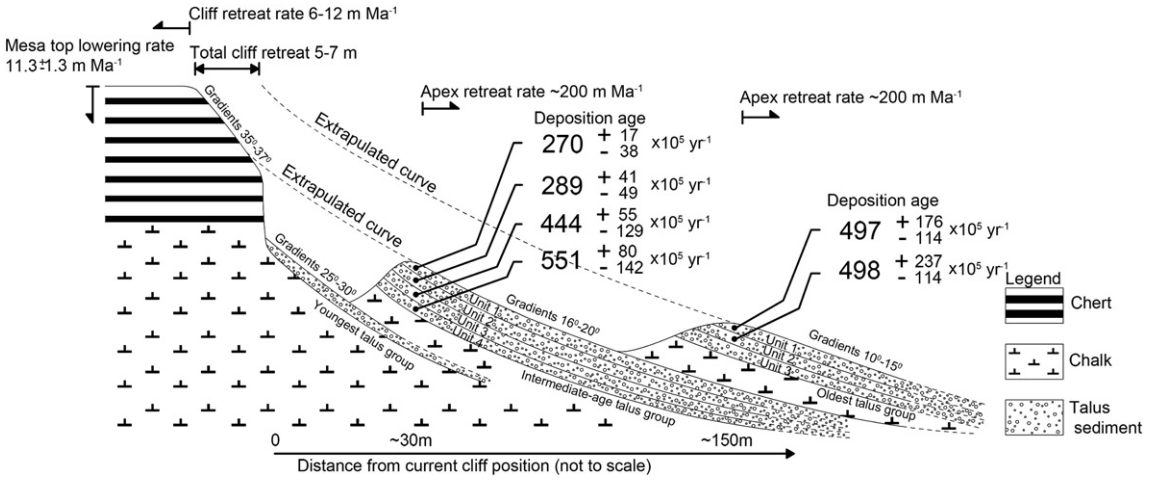

Figure 6. Schematic sketch of the talus flatiron sequences in the study area including talus depositional units, model ages of deposition, rates and magnitude of geomorphic processes, talus and cliff gradients and extrapolated curves of their surfaces.

inheritance of the older talus group could theoretically reflect (a) significant differences in paleo-erosion rates of cliffs and catchments (e.g. Anderson et al., 1996; Granger et al., 1996) between the oldest and the intermediate-age talus groups (Fig. 7c) or (b) significant differences in the pre-deposition exposure duration of clasts (e.g. Hancock et al., 1999) as a function of the distance from the source of sediments (Fig. 7d). In practice, however, there is no evidence for major climatic shifts (see discussion below) to support a temporal shift as described in (a). In addition, significant temporal changes in retreat rates and inheritance cannot be ascribed to a decrease of the mesa-top area, as this area hardly changed since the deposition of the older talus (the calculated cliff retreat rates are only 6–12 m/Ma (Boroda et al., 2011)). The concentration of ^{10}Be in bedrock samples collected from the cliffs of Tzuk Tamrur (sample TTSL1) is similar to that of Giva't Zeron (samples ZRSL1 and ZRSL2; Boroda et al., 2011) of which the mesa top area is much smaller. This could suggest that under hyperarid conditions the area of the mesa does not play an important role in setting the cliff-retreat rate and that the rate of cliff retreat has not changed much over the time of the formation of the talus groups at Giva't Zeron (Fig. 6). The difference in the modeled average inheritance values

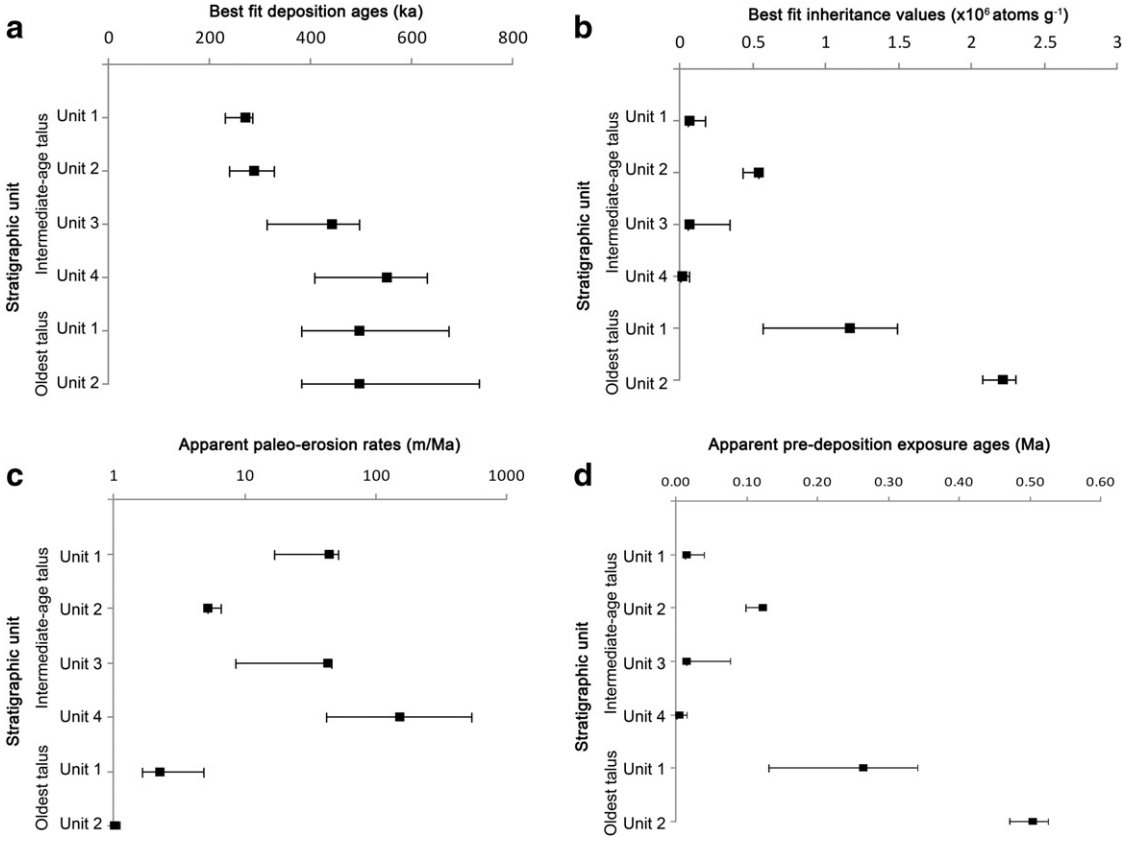

Figure 7. Best-fit model results for the stratigraphic units composing the intermediate-age talus group and the oldest talus group. (a) Deposition ages (ka). (b) Inheritance ($\times 10^6$ atoms g^{-1}). (c) Apparent paleo-erosion rates (m/Ma) for Giva't Zeron mesa which could potentially reflect significant changes in cliff-retreat rates or catchment-denudation rates with time. (d) Apparent pre-deposition exposure duration (Ma) which could potentially reflect differences in the clasts transport time as a function of the distance from the source of sediments.

https://doi.org/10.1016/j.yqres.2012.11.012 Published online by Cambridge University Press

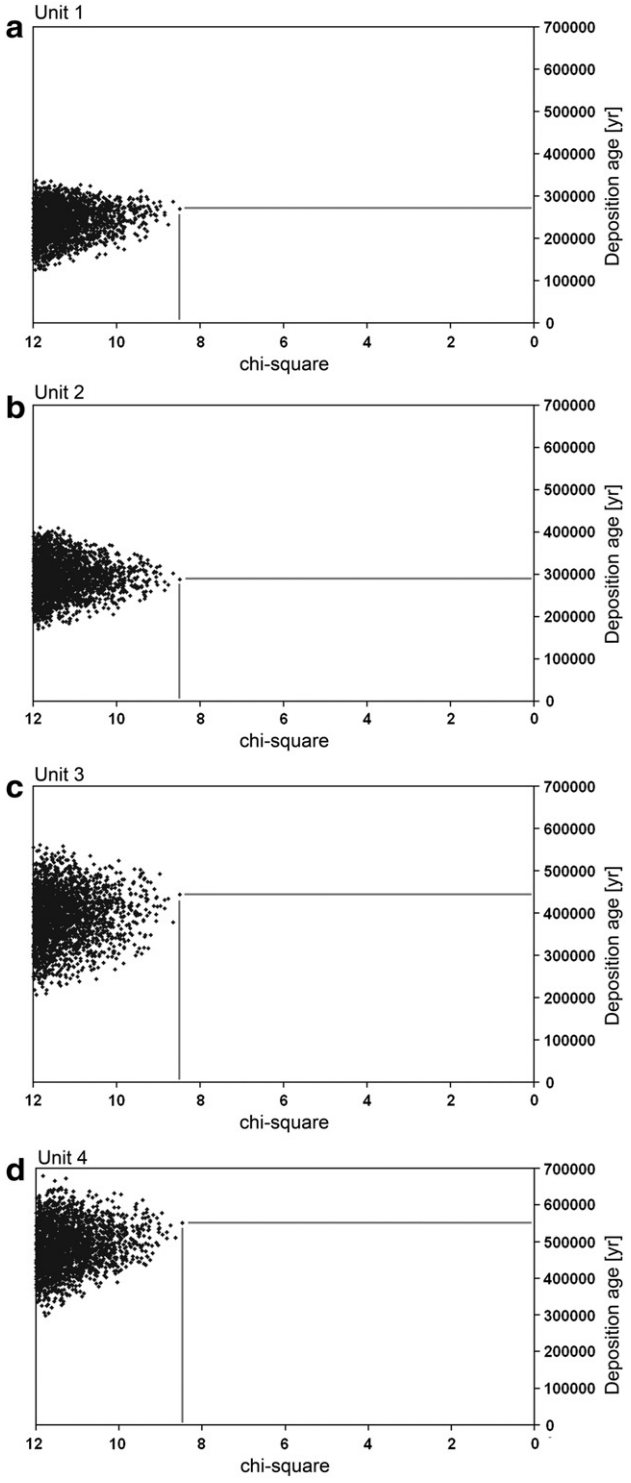

Figure 8. The age solution space for four depositional events composing profile ZRBE. Horizontal lines indicate the model best age and a vertical line indicates the corresponding chi-square value. Note that the spread in the ages decreases as the minimum chi-square is approached.

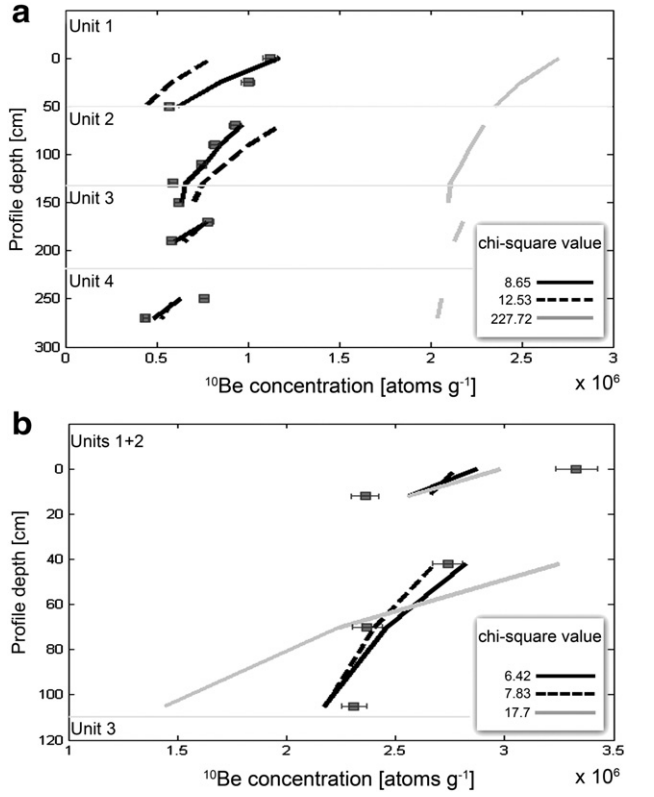

Figure 9. Concentration vs. depth plot showing measured ^{10}Be concentrations (gray squares) and the best-fit calculated ^{10}Be profile (black line) for (a) Intermediate-age talus group (trench ZRBE) and (b) Oldest talus group (trench ZRAF). Dashed lines represent the model results when forcing constant inheritance and the gray lines represent the model results when applying the average inheritance from the other talus group. The best-fit predicted profile is based on more than 10^9 model runs. Gray horizontal lines indicate the contacts between colluvial units.

between the two talus groups can therefore be attributed mostly to the transport distance (30 vs. 150 m for the intermediate-age and oldest talus group respectively) and the duration of exposure during transport (Fig. 7d). Although the soil stratigraphy of all the talus groups indicates that the regional climatic conditions were consistently hyperarid to arid, some temporal variability in cliff retreat rates and mesa-top erosion rates due to non-steady climatic parameters cannot be ruled out.

The observed variability in the inheritance values among the different units of a single talus flatiron most probably represents the stochastic nature of sediment production and transport on slopes in this hyperarid environment. Factors that may contribute to the stochastic nature of inheritance include variation in the amount and intensity of precipitation events and overland flow (Yair and Lavee, 1985), the mode and rate of cliff disintegration (Douglas et al., 1991; Haviv et al., 2010), the grain size of the sediment being transported, the specific transport mechanism, and the depth of mixing during transport.

The evolution of the talus–cliff couplet in the hyperarid Negev

The results described above combined with those presented in Boroda et al. (2011) contribute to the understanding of the depositional history of talus flatirons and transport processes of sediment on slopes. Initially, the cliff face acted as a source for clasts, which accumulated on the bedrock slope and formed a relatively smooth talus deposit that stretched from the free-face of the cliff to the pediment. Accumulation occurred in several stages. Successive stages are marked by deposition of a new layer of clasts upon the previously accumulated talus deposit. The transport rate of each deposit varied significantly due to reasons noted in the previous section. The process of deposition continued until active rills and gullies detached the talus deposits from its source cliff (at 497 $^{+176}_{-114}$ ka, for the oldest talus group) and terminated its sediment supply. Following the detachment and abandonment of the old talus, the formation of new talus begun at 551 $^{+80}_{-142}$ ka. The intermediate-age talus group experienced a similar process and was detached and abandoned at 270 $^{+17}_{-38}$ ka (Fig. 6). This temporal framework indicates that the development of the

https://doi.org/10.1016/j.yqres.2012.11.012 Published online by Cambridge University Press

studied talus sequences is not specifically associated with Pleistocene glacial–interglacial cycles as was proposed for semiarid and hyperarid deserts. For example, in a semiarid region of Spain, radiocarbon ages were used to correlate between talus deposition phases and short cool events such as Heinrich events and late Holocene neoglaciations (Gutiérrez et al., 2006) and short intervals of 2.5–25 ka between successive talus generations were proposed. Gerson (1982) and Gerson and Grossman (1987) hypothesized, without rigorous geochronologic constraints on colluvial or related alluvial deposits, that such sequences were caused by hyperarid to semi-arid climate changes on time scales of about 100 ka. However, the soils and the paleosols in our study site are all gypsic and saline soils, which indicate hyperarid climate conditions since the initial stages of talus formation; i.e. at least since the early Pleistocene (Dan and Yaalon, 1982; Amit and Gerson, 1986; Amit and Yaalon, 1996; Amit et al., 2006). Even weakly developed calcic horizons that typically form in wetter regions of the Negev area (>80 mm yr^{-1}, Amit et al., 2006, 2010) are not observed in the soils in the study area. The ages of the dust in the soil, determined by OSL, reflect relatively young stages of dust accumulation. These ages which represent minimum ages for the talus deposits (Boroda et al., 2011) combined with the degree of soil development are similar to those found on middle to late Pleistocene alluvial surfaces in the region (Dan and Yaalon, 1982; Amit and Gerson, 1986; Amit and Yaalon, 1996) and are in accordance with the main period of loess deposition in the Negev (~14–180 ka; Crouvi et al., 2008, 2009).

Moreover, we suggest that talus formation and abandonment is not necessarily associated with fast cliff retreat (Fig. 6). The results of this study support the conclusions reported in Boroda et al. (2011). They concluded that the slow cliff-retreat rates inferred on the basis of cosmogenic isotopes exposure ages dating in this region (6–12 m/Ma) did not support the model proposed by Gerson (1982) that requires periods of rapid cliff retreat to produce the observed significant separation of the cliffs and talus flatirons. Instead, we propose that the talus flatirons retreat from the cliffs at a rate of about ~200 m/Ma (Fig. 6). We also hypothesize that this retreat is the result of substantial gully erosion favored by the soft chalk exposed beneath the talus, and the unconsolidated nature of the talus (Boroda et al., 2011). We propose that talus-apex retreat rate decreases as its distance from the cliff increases due to decrease in talus gradient, increase in the colluvium thickness and increase of the armoring of the talus desert pavement with time. These processes explain the concentric position of the different generations of the talus flatirons around the cliff.

Conclusions

Sedimentary and soil profiles of two generations of talus flatirons have been documented in the hyperarid environment of Giva't Zeron and Tzuk Tamrur in the northeastern Negev. The stratigraphy of the intermediate-age talus flatirons group includes four colluvial units separated by three buried soils. The stratigraphy of the oldest flatirons group includes at least three colluvial units. The presence of soils between the depositional units in each talus group and ^{10}Be concentration distribution with depth indicates negligible erosion of the surface layer between successive depositional events. Numerical modeling of cosmogenic isotope depth profiles indicates that the intermediate-age talus group first depositional event occurred at 551 $^{+80}_{-142}$ ka and its abandonment and stabilization occurred at 270 $^{+17}_{-38}$ ka. The abandonment and stabilization of the upper units of the oldest talus group occurred at 497 $^{+176}_{-114}$ ka. This temporal framework indicates that the development of the studied talus sequences is not specifically associated with Pleistocene glacial–interglacial cycles. The ages of the soil dust fraction dated by OSL reflect a late stage of soil formation which followed dust accumulation. These ages are in accordance with the main period of loess deposition in the Negev (~14–180 ka). Our numerical modeling also reveals large variability in inheritance values among the units composing each talus flatiron and significant inheritance differences between talus flatirons of different groups. We suggest that the variability in inheritance values among different units within the same talus flatiron deposit reflect the stochastic nature of sediment transport on relatively steep slopes in hyperarid environments and the stochastic nature of sediment production from the associated cliffs. The prominent inheritance differences between the talus flatirons of different groups can be attributed mostly to the transport distance and duration of gravel exposure.

Acknowledgments

This research was supported by the Israel Science Foundation grant 146/08, the United States–Israel Binational Science Foundation grant 2006-221 and the U.S. Army Research Office grant (DAAD19-03-1-0159). We thank Y. Rephael and A. Muskin for field assistance, Y. Nahmias and S. Mazeh for lab assistance, N. Teutsch for performing the ICP-OES analysis, A. Boroda for figure editing, and E. Morin, M. Tsaserski and Y. Amiel for fruitful discussion. We thank K. Nichols, L. McFadden, B. Harrison, R. Braucher, and A. Gillespie for their thoughtful comments that significantly improved this paper.

References

Aitken, M.J., 1998. An Introduction to Optical Dating. Oxford University Press, Oxford.
Amit, R., Gerson, R., 1986. The evolution of Holocene Reg (gravelly) soils in deserts – An example from the Dead Sea region. Catena 13, 59–79.
Amit, R., Gerson, R., Yaalon, D.H., 1993. Stages and rate of gravel shattering process by salts in desert Reg soils. Geoderma 57, 295–324.
Amit, R., Yaalon, D.H., 1996. Micromorphology of gypsum and halite in Reg soils—The Negev Desert, Israel. Earth Surface Processes and Landforms 21, 1127–1143.
Amit, R., Enzel, Y., Sharon, D., 2006. Permanent Quaternary hyperaridity in the Negev, Israel, resulting from regional tectonics blocking Mediterranean frontal systems. Geology 34, 509–512.
Amit, R., Enzel, Y., Grodek, T., Couvi, O., Porat, N., Ayalon, A., 2010. The role of rare rainstorms in the formation of calcic soil horizons on alluvial surfaces in extreme deserts. Quaternary Research 74, 177–187.
Anders, M.D., Pederson, J.L., Rittenour, T.M., Sharp, W.D., et al., 2005. Pleistocene geomorphology and geochronology of eastern Grand Canyon: linkages of landscape components during climate changes. Quaternary Science Review 24, 2428–2448.
Anderson, R.S., Repka, J.L., Dick, G.S., 1996. Explicit treatment of inheritance in dating depositional surfaces using in situ ^{10}Be and ^{26}Al. Geology 59, 47–51.
Arauzo, T., Gutiérrez, M., Sancho, C., 1996. Facetas triangulares de ladera como indicadores paleoclimàticos en ambientes semi'aridos Depresión del Ebro. Geogaceta 20, 1093–1095.
Balco, G., Stone, J.O., Lifton, N.A., Dunai, T.J., 2008. A complete and easily accessible means of calculating surface exposure ages or erosion rates from ^{10}Be and ^{26}Al measurements. Quaternary Geochronology 3, 174–195.
Bevington, P.R., Robinson, D.K., 2003. Data Reduction and Error Analysis for the Physical Sciences, 3rd ed. McGraw-Hill, Boston.
Bierman, P.R., Turner, J., 1995. ^{10}Be and ^{26}Al evidence for exceptionally low rates of Australian bedrock erosion and the likely existence of pre-Pleistocene landscapes. Quaternary Research 44, 378–382.
Bierman, P.R., Caffee, M., 2001. Steady state rates of rock surface erosion and sediment production across the hyper-arid Namib Desert and the Namibian escarpment, Southern Africa. American Journal of Science 301, 326–358.
Birkeland, P.W., 1999. Soils and Geomorphology. Oxford University Press, Oxford.
Boroda, R., Amit, R., Matmon, A., Team, A.S.T.E.R., Finkel, R., Porat, N., Enzel, Y., Eyal, Y., 2011. Quaternary-scale evolution of sequences of talus flatirons in the hyperarid Negev. Geomorphology 127, 41–52.
Braucher, R., Del C, P., Siame, L., Hidy, A.J., Bourles, D.L., 2009. Determination of both exposure time and denudation rate from an in situ-produced ^{10}Be depth profile: a mathematical proof of uniqueness. Model sensitivity and applications to natural cases. Quaternary Geochronology 4, 56–67.
Brocard, G.Y., van der Beek, P.A., Bourles, D.L., Siame, L.L., Mugnier, J.L., 2003. Long-term flivial incision rates and postglacial river relaxation time in the French Western Alps from ^{10}Be dating of alluvial terraces with assessment of inheritance, soil development and wind ablation effects. Earth and Planetary Science Letters 209, 197–214.
Brown, E.T., Bourles, D.L., Burchfiel, B.C., Qidong, D., Jun, L., Molnar, P., Raisbeck, G.M., Yiou, F., 1998. Estimation of slip rates in the southern Tien-Shan using cosmic ray exposure dates of abandoned alluvial surfaces. Geological Society of America Bulletin 110, 377–386.
Bull, W.B., 1991. Geomorphic Response to Climatic Change. Oxford University Press, Oxford.
Carson, M.A., Kirkby, M.J., 1972. Hillslope Form and Process. Cambridge University Press, Cambridge.

https://doi.org/10.1016/j.yqres.2012.11.012 Published online by Cambridge University Press

Crouvi, O., Amit, R., Enzel, Y., Porat, N., Sandler, A., 2008. Sand dunes as a major proximal dust source for late Pleistocene loess in the Negev Desert, Israel. Quaternary Research 70, 275–282.
Crouvi, O., Amit, R., Porat, N., Gillespie, A.R., McDonald, E.V., Enzel, Y., 2009. Significance of primary hilltop loess in reconstructing dust chronology, accretion rates, and sources; an example from the Negev Desert, Israel. Journal of Geophysical Research- Earth Surface 114, F02017.
Dan, J., Yaalon, D.H., 1982. Automorphic saline soils in Israel. In: Yaalon, D.H. (Ed.), Aridic Soils and Geomorphic Processes: Catena Supplement, 1, pp. 103–115 (Reiskirchen).
Dan, J., Raz, Z., Koyumdjisky, H., 1964. Soil Survey Manual: Division of Scientific Publication. The Volcani Center, Bet Dagan, Israel . (in Hebrew).
Dorn, R., 1983. Cation-ratio dating: a new rock varnish age determination technique. Quaternary Research 20, 49–73.
Douglas, G.R., Whalley, W.B., McGreevy, J.P., 1991. Rock properties as controls on free-face debris fall activity. Permafrost and Periglacial Processes 2, 311–319.
Enzel, Y., Amit, R., Grodek, T., Ayalon, A., Lekach, J., Porat, N., Bierman, P., Blum, J.D., Erel, Y., 2012. Late Quaternary weathering, erosion, and deposition in Nahal Yael, Israel: An "impact of climatic change on an arid watershed"? Geological Society of America Bulletin 124, 705–722.
Everard, C.E., 1963. Contrasts in the form and evolution of hill-side slopes in central Cyprus. Transactions of the Institute of British Geographers 32, 331–347.
Gerson, R., 1982. Talus relicts in deserts: a key to major climatic fluctuations. Israel Journal of Earth Science 31, 123–132.
Gerson, R., Grossman, S., 1987. Geomorphic activity on escarpment and associated fluvial systems in hot deserts as an indicator of environmental regimes and eyclic climatic changes. In: Rarmpino, M.R., Sanders, J.E., Newman, W.S., Koningsson, L.K. (Eds.), Climate: History, Periodicity, Predictability. Van Nostrand Reinhold, Stroudsburg, PA, pp. 301–322.
Gosse, J.C., Phillips, F.M., 2001. Terrestrial in situ cosmogenic nuclides: theory and application. Quaternary Science Reviews 20, 1475–1560.
Granger, D.E., Muzikar, P.F., 2001. Dating sediment burial with in situ-produced cosmogenic nuclides; theory, techniques, and limitations. Earth and Planetary Science Letters 188, 269–281.
Granger, D.E., Smith, A.L., 2000. Dating buried sediments using radioactive decay and muogenic production of ^{26}Al and ^{10}Be. Nuclear Instruments and Methods in Physics Research 172, 822–826.
Granger, D.E., Kirchner, J., Finkel, R., 1996. Spatially averaged long-term erosion rates measured from in situ-produced cosmogenic nuclides in alluvial sediment. Journal of Geology 104, 249–257.
Guralnik, B., Matmon, A., Avni, Y., Fink, D., 2010. ^{10}Be exposure ages of ancient desert pavements reveal Quaternary evolution of the Dead Sea drainage basin and rift margin tilting. Earth and Planetary Science Letters 290, 132–141.
Gutiérrez, M., Martinez, V.H., 2001. Multiple talus flatirons, variation of cliff retreat rates and the evolution of slopes in Almazan Basin (semi-arid central Spain). Geomorphology 38, 19–29.
Gutiérrez, M., Sancho, C., Arauzo, T., 1998. Cliff retreat rates in semiarid environments from talus flatirons, Ebro Basin, NE Spain. Geomorphology 25, 111–121.
Gutiérrez, M., Gutiérrez, F., Desir, G., 2006. Considerations on the chronological and causal relationships between talus flatirons and palaeoclimatic changes in central and northeastern Spain. Geomorphology 73, 50–63.
Hancock, G., Anderson, R., Chadwick, O., Finkel, R., 1999. Dating fluvial terraces with ^{10}Be and ^{26}Al profiles: application to the Wind River, Wyoming. Geomorphology 27, 41–60.
Haviv, I., Enzel, Y., Whipple, K.X., Zilberman, E., Matmon, A., Stone, J., Fifield, K.L., 2010. Evolution of vertical knickpoints (waterfalls) with resistant caprock; insights from numerical modeling. Journal of Geophysical Research 115, F3.
Hidy, A., Gosse, J., Pederson, J., Mattern, P., Finkel, R., 2010. A geologically constrained Monte Carlo approach to modeling exposure ages from profiles of cosmogenic nuclides: an example from Lees Ferry, Arizona. Geochemistry, Geophysics, Geosystems 11.
Howard, A.D., Selby, M.J., 1994. Rock slopes. In: Abrahams, A.D., Parsons, A.J. (Eds.), Geomorphology of Desert Environments. Chapman & Hall, London, pp. 123–172.
Koons, D., 1955. Cliff retreat in the southwestern United States. American Journal of Science 253, 44–52.
Korschinek, G., Bergmaier, A., Faestermann, T., Gerstmann, U.C., Knie, K., R7ugel, G., Wallner, A., Dillmann, I., Dollinger, G., von Gostomski, Ch. Lierse, Kossert, K., Maitia, M., Poutivtsev, M., Remmert, A., 2010. A new value for the half-life of ^{10}Be by Heavy-Ion Elastic Recoil Detection and liquid scintillation counting. Nuclear Instruments and Methods in Physics Research B 286, 187–191.
Lal, D., Arnold, J., 1985. Tracing quartz through the environment: proceeding of Indian Academic Science. Earth and Planetary Science Letters 94, 1–5.
Lal, D., 1991. Cosmic ray labeling of erosion surfaces: In situ production rates and erosion models. Earth and Planetary Science Letters 104, 424–439.
Matmon, A., Simhai, O., Amit, R., Haviv, I., Enzel, Y., Porat, N., McDonald, E.V., Benedetti, L., Finkel, R.C., 2009. Desert pavement-coated surfaces in extreme deserts present the longest-lived landforms on Earth. Geological Society of America Bulletin 121, 688–697.
Matsushi, Y., Wakasa, S., Matsuzaki, H., Matsukura, Y., 2006. Long-term denudation rates of actively uplifting hillcrests in the Boso Peninsula, Japan, estimated from depth profiling of in situ-produced cosmogenic ^{10}Be and ^{26}Al. Geomorphology 82, 283–294.
Murray, A.S., Wintle, A.G., 2000. Luminescence dating of quartz using improved single-aliquot regenerative-dose protocol. Radiation Measurements 32, 57–73.
Nichols, K.K., Bierman, P.R., Hooke, R.L., Clapp, E.M., Caffee, M., 2002. Quantifying sediment transport on desert piedmonts using ^{10}Be and ^{26}Al. Geomorphology 45, 105–125.
Nichols, K., Bierman, P., Eppes, M., Caffee, M., Finkel, R., Larsen, J., 2005. Deciphering the Late Pleistocene and Holocene history of the complex Chemehuevi Mountain piedmont using 10Be and 26Al. American Journal of Science 305, 345–368.
Nichols, K., Bierman, P., Foniri, W., Gillespie, A., Caffee, M., Finkel, R., 2006. Dates and rates of arid region geomorphic processes. GSA Today 16, 4–11.
Nishiizumi, K., Imamura, M., Caffee, M.W., Southon, J.R., Finkel, R.C., McAninch, J., 2007. Absolute calibration of ^{10}Be AMS standards. Nuclear Instruments and Methods in Physics Research B 258, 403–413.
Pederson, J.L., Smith, G., Pazzaglia, F., 2001. Comparing the modern, Quaternary, and Neogene records of climate controlled hillslope sedimentation in southeast Nevada. Geological Society of America Bulletin 113, 305–319.
Perg, L.A., Anderson, R.S., Finkel, R.C., 2001. Use of a new ^{10}Be and ^{26}Al inventory method to date marine terraces, Santa Cruz, California, USA. Geology 29, 879–882.
Phillips, M.P., McDonald, E.V., Reneau, S.L., Poths, J., 1998. Dating soils and alluvium with cosmogenic 21Ne depth profiles: case studies from the Pajarito Plateau, New Mexico, USA. Earth and Planetary Science Letters 160, 209–223.
Porat, N., 2007. (TR-GSI/2/2002) Analytical Procedures in the Luminescence Dating Laboratory. Geological Society of Israel, Jerusalem, Israel, p. 33 (in Hebrew).
Riihimaki, C.A., Anderson, R.S., Safran, E.B., Dethier, D.P., Finkel, R.C., Bierman, P.R., 2006. Longevity and progressive abandonment of the Rocky Flats surface, Front Range, Colorado. Geomorphology 78, 265–278.
Sancho, C., Gutiérrez, M., Pene, J.L., Burillo, F., 1988. A quantitative approach to cliff retreat starting from triangular slope facets, central Ebro Basin, Spain. Catena Supplement 13, 139–146.
Schmidt, K.H., 1994. Hillslopes as evidence of climate change. In: Abrahams, A.D., Parsons, A.J. (Eds.), Geomorphology of Desert Environments. Chapman & Hall, London, UK, pp. 553–570.
Schmidt, K.H., 1996. Talus and pediment flatirons-indicators of climatic change on cliff slope on the Colorado Plateau, USA. Zeitschrift fur Geomorphology 103, 135–158.
Shaw, S.H., 1947. Geological Map of Southern Palestine, with explanatory notes: Jerusalem, Govt. of Palestine, 42 pp.
Small, E.E., Anderson, R.S., Hancock, G.S., 1999. Estimates of the rate of regolith production using ^{10}Be and ^{26}Al from an alpine hillslope. Geomorphology 27, 131–150.
Soil Survey Staff, 1975. Soil taxonomy. Agriculture Handbook. U.S Department of Agriculture, Soil Conservation Service.
Stone, J., 2000. Air pressure and cosmogenic isotope production. Journal of Geophysical Research 105, 23,753–759.
Yair, A., Lavee, H., 1985. Runoff generation in arid and semi-arid zones. In: Anderson, M.G. (Ed.), Hydrological Forecasting. John Wiley and Sons, New York, pp. 183–220.

https://doi.org/10.1016/j.yqres.2012.11.012 Published online by Cambridge University Press